

# Finite-bandwidth effects in strong-field ionization of atoms by few-cycle circularly polarized laser pulses

C. P. J. Martiny and L. B. Madsen

*Lundbeck Foundation Theoretical Center for Quantum System Research, Department of Physics and Astronomy, University of Aarhus, 8000 Århus C, Denmark*

(Received 6 June 2007; published 16 October 2007)

In the strong-field approximation, we calculate the electron momentum distribution following strong-field ionization of atomic hydrogen by an  $N$ -cycle circularly polarized laser pulse. For  $N \leq 5$ , our results show a pronounced interference structure in addition to the well-known carrier-envelope phase difference (CEPD) sensitivity. With increasing  $N$  we observe a gradual change to a momentum distribution which is free of interference and CEPD effects and which is characterized by well-resolved above-threshold ionization peaks, consistent with the quantized photon picture. The changes in the interference structures are explained by the spectral properties of the pulse. We compare the results of the strong-field approximation with those obtained by the saddle-point method and show that while the saddle-point method is able to reproduce the results for  $N \geq 5$ , it fails to explain the interference structure and the asymmetry of the distribution for smaller  $N$ .

DOI: [10.1103/PhysRevA.76.043416](https://doi.org/10.1103/PhysRevA.76.043416)

PACS number(s): 32.80.Rm, 42.50.Hz

## I. INTRODUCTION

Nowadays, intense laser pulses with only a few optical cycles are available in several laser laboratories (see, for instance, Ref. [1] and references therein). Such pulses can be used to probe molecular and atomic dynamics on a very short time scale [2,3]. For example, few-cycle pulses together with a subfemtosecond soft x-ray pulse were used to study atomic physics on an attosecond time scale [4–6], nuclear dynamics in molecules was investigated with few-cycle pulses using high harmonics generation [7], and few-cycle laser pulses were used to obtain an image of an electronic orbital [8].

Another field, which is expected to benefit highly from the development of few-cycle laser pulses is coherent control. It was, e.g., recently demonstrated experimentally [9] that few-cycle pulses can be used to control dissociative ionization of  $D_2$ —i.e., control reaction dynamics. Coherent control with few-cycle pulses has also been studied in a number of theoretical papers [10,11]. The essential parameter in coherent control with few-cycle pulses is the carrier-envelope phase difference (CEPD) of the pulse. A long monochromatic pulse is completely characterized by the frequency, amplitude, and polarization. A few-cycle pulse, on the other hand, requires additional parameters: the carrier-envelope phase difference and the number of optical cycles. This leads to new effects in laser-matter interactions—e.g., strong CEPD dependence of the direction of ejection of an electron in the ionization process and finite-bandwidth effects (see, e.g., Refs. [12–20] and references therein). For linearly polarized pulses, where the extrema of the field are relatively well localized, the CEPD dependence in ionization may be understood by the approximate exponential dependence of the ionization rate on the instantaneous field strength, which means that the electron most likely escapes at the instants of time where the carrier attains local extrema within the envelope [1]. The situation is quite different for circularly polarized pulses. In this case the extrema are less localized temporally and the field may change its direction by at least  $\pi/2$

while having almost maximum strength (see Figs. 1 and 2 below). As a consequence the momentum distributions are quite broad even for a two-cycle pulse. For atomic and molecular systems with a field-free Hamiltonian which is invariant under rotations around the propagation direction of the circularly polarized few-cycle pulse a characterization of CEPD effects for changing values of this phase was recently given [19] in terms of a corresponding rotation of the total system around the propagation direction. CEPD effects only occur for very short pulses [16], which means that we are in the regime where bandwidth effects are expected to be important.

Although considerable research has been devoted to CEPD effects, not much attention has been paid to the related question of bandwidth effects. The purpose of the present paper is twofold. First, we want to study the effects of the finite bandwidth of a few-cycle pulse on the electron momentum distribution in the strong-field ionization of atoms. Second, we investigate to what extent a very popular approach within the strong-field approximation (SFA)—the saddle-point method (SPM)—accounts for all the structure in the electron momentum distribution when the number of optical cycles within the pulse is varied. More precisely, we investigate how the momentum distribution for atomic hydrogen depends on the number of optical cycles—i.e., the pulse length. The consideration of H as the system for our investigation is for computational convenience and not a restriction when it comes to an identification of the generic physics since bandwidth and CEPD effects are related to the characteristics of the pulse more than to the particular atomic (or molecular) system.

The paper is organized as follows. In Sec. II we review the SFA and the SPM. In Sec. III we discuss the results. Section IV concludes.

## II. THEORY

In the following we consider atomic hydrogen interacting with a field described by the right-hand circularly polarized vector potential  $\vec{A}$ ,

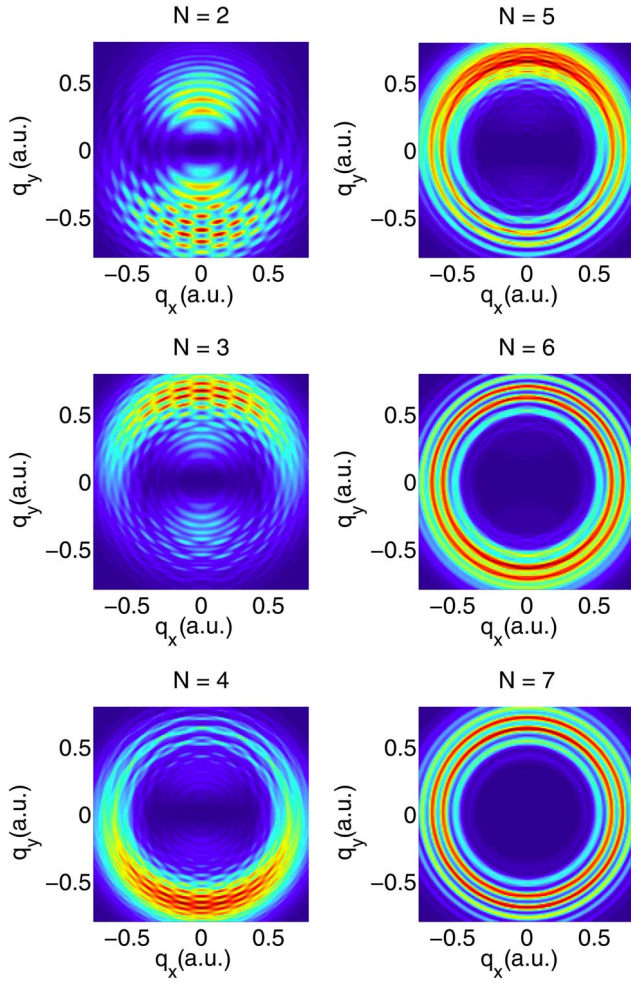


FIG. 1. (Color online) Momentum distribution  $(q_x, q_y)$  calculated using Eqs. (1) and (2) in the plane of polarization of the right-hand circularly polarized field  $\vec{E}$  propagating in the  $z$  direction for strong-field ionization of H(1s) for various values of  $N$ , with  $I = 5.0 \times 10^{13}$  W/cm<sup>2</sup>,  $\omega_0 = 0.057$  (800 nm), and  $\phi = \pi/2$ . The grid size is  $\Delta q_x = \Delta q_y = 0.01$ .

$$\vec{A}(t) = \frac{f(t)A_0}{\sqrt{2}} [\cos(\omega_0 t + \phi)\vec{e}_x + \sin(\omega_0 t + \phi)\vec{e}_y]$$

for  $t \in [0; \tau]$  and  $\vec{A} = \vec{0}$  otherwise. Here  $A_0$  is the amplitude,  $\tau$  is the pulse length,  $\omega_0$  is the carrier frequency,  $f(t) = \sin^2[\omega_0 t / (2N)]$  is the envelope, with  $N$  the number of optical cycles, and  $\phi$  the CEPD. The corresponding electric field is obtained as  $\vec{E} = -\partial_t \vec{A}$  [we use atomic units ( $\hbar = |e| = a_0 = m_e = 1$ ) throughout].

In the SFA [21–24] the probability amplitude for direct ionization is given by

$$T_{fi} = -i \int_0^\tau \langle \Psi_f(t) | V(t) | \Psi_i(t) \rangle dt, \quad (1)$$

with  $\Psi_i$  the initial wave function,  $\Psi_f$  the final continuum wave function, and  $V(t) = \vec{r} \cdot \vec{E}(t)$  the length gauge interaction operator (see, e.g., Refs. [25–28] for recent references dis-

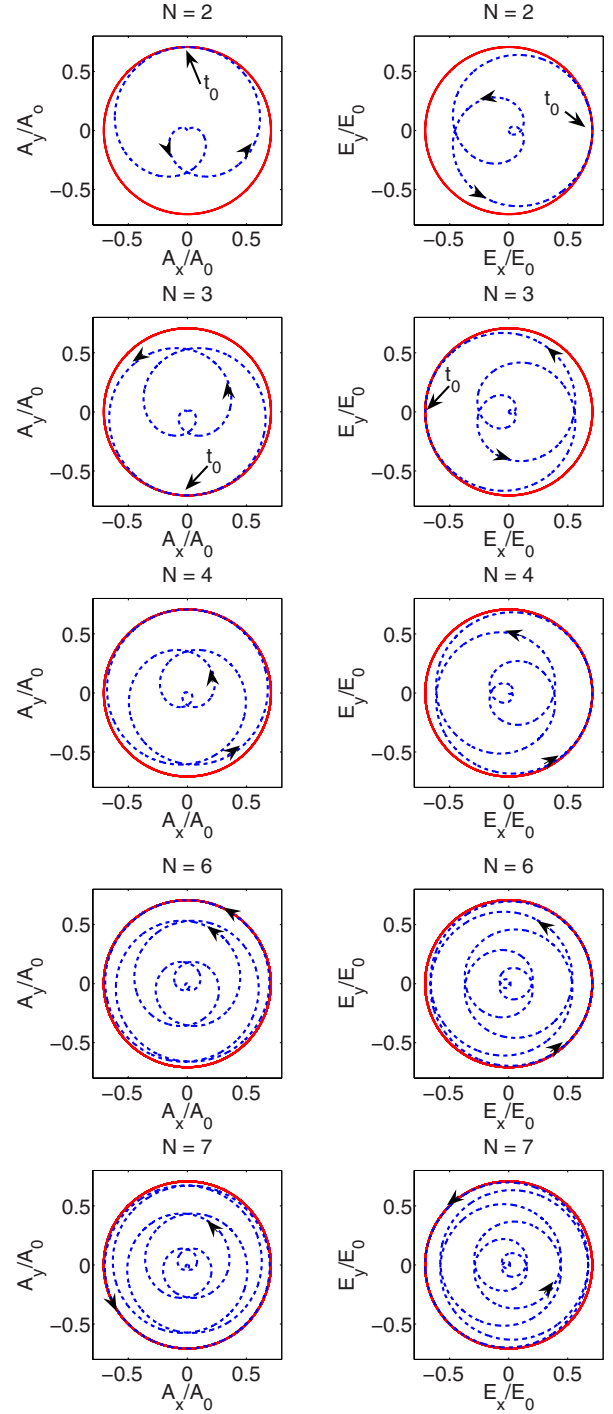


FIG. 2. (Color online) Vector potential and electric field (blue dotted line) for five different values of  $N$ . The solid curve shows the carrier wave—i.e., the field without the envelope. The arrows show the natural time evolution for the pulse. The parameters are  $I = 5.0 \times 10^{13}$  W/cm<sup>2</sup>,  $\omega_0 = 0.057$  (800 nm), and  $\phi = \pi/2$ .

cussing the choice of gauge). The initial state of the system is assumed to be the atomic ground state H(1s). The final state is represented by a Volkov wave function. The Volkov state describes the state of a free electron in an electromagnetic field, so in this state the Coulomb potential is completely neglected.

The momentum distribution of the ejected electron is given by the absolute square of the probability amplitude, and integrating over  $q_z$  gives us the  $(q_x, q_y)$  momentum distribution in the plane of polarization of the circularly polarized light:

$$\frac{dP}{dq_x dq_y} = \int_{-\infty}^{\infty} |T_{fi}|^2 dq_z. \quad (2)$$

The spatial integration in Eq. (1) can be performed analytically, so we are left with a one-dimensional time integral which we evaluate numerically by quadrature as detailed in Sec. III.

In Sec. III, we shall first be concerned with a discussion of results obtained on the basis of Eq. (1) with direct numerical integration, and second we shall investigate to what extent the SPM described below is capable of accounting for all the structures in the spectra.

For multiphoton processes the matrix element in Eq. (1) contains a very rapidly oscillating phase factor  $\exp[iS(t)]$ . In the case when the final state is described by a Volkov state, this phase reads  $S(t) = \frac{1}{2} \int_0^t [\vec{q} + \vec{A}(t')]^2 dt' + I_p t$ , with  $\vec{q}$  the asymptotic momentum and  $I_p$  the ionization potential. One may therefore use the SPM to calculate an approximate value for the integral (1) [20]. Besides its computational convenience, the SPM also gives physical insight since it provides a time analysis of the results obtained [see Eqs. (3) and (4) below]. These features make the SPM very popular for calculating transition amplitudes in strong-field physics, and it has been used to describe a number of physical processes including ionization [15], high harmonics generation [29], and rescattering [18]. The SPM gives the following expression for  $T_{fi}$  [20]:

$$T_{fi} = -\frac{1}{\sqrt{2}} \sum_{t_s} a_s(t_s) \exp[iS(t_s)], \quad (3)$$

where  $a_s$  are complex amplitudes given explicitly for H(1s) [20],  $a_s(t_s) = 1/S''(t_s)$ , and the instants of time  $t_s$  are solutions to the saddle-point equation

$$\frac{\partial S}{\partial t}(t_s) = 0. \quad (4)$$

For a circularly polarized laser pulse with  $N$  optical cycles, there are  $N+1$  solutions for  $t_s$  [20]. The solutions are typically complex since ionization is a classically forbidden process except in the over-the-barrier regime.

### III. RESULTS AND DISCUSSION

Figure 1 presents the calculated momentum distribution for different numbers of optical cycles  $N$ , with  $I = 5.0 \times 10^{13}$  W/cm<sup>2</sup>,  $\omega_0 = 0.057$  (800 nm), and  $\phi = \pi/2$ . The integral in Eq. (1) is calculated using Gauss-Legendre quadrature [30], while the integral over  $q_z$  is calculated using an equidistant grid on  $[-Q_z, Q_z]$ , where  $Q_z$  is chosen large enough to ensure convergence,  $Q_z = 0.6$  in the present case. For  $N \leq 5$  we observe (i) a well-known asymmetry in the direction of electron ejection [12–20] (see Sec. III A) and (ii) a compli-

cated interference pattern radially as well as angularly (see Sec. III B).

#### A. CEPD effect

In Fig. 1, we see how the CEPD effect disappears for increasing number of optical cycles of the ionizing pulse. We include a brief discussion of this well-known effect for completeness. The preferred direction of electron emission is a CEPD effect and can be explained classically by assuming that an electron is freed at the peak of the field  $t = t_0$  with initial velocity  $\vec{v}(t_0) = \vec{0}$  and subsequently moves under the influence of the external field only [16,19],

$$\vec{q}_{\text{final}} = - \int_{t_0}^{\infty} \vec{E}(t') dt' = -\vec{A}(t_0). \quad (5)$$

Hence, the direction of ejection is opposite the direction of the maximum vector potential. Notice that this equation is the saddle-point equation in the strong-field limit, where we can neglect the ionization potential. Figure 2 shows the vector potential and the corresponding electric field for five different values of  $N$ . For  $N = 2, 3, 4$  we observe a good agreement between this simple model and the quantum results in Fig. 1. The momentum distributions for other values of the CEPD  $\phi$  are obtained by a simple rotation of the momentum spectra by  $\phi - \pi/2$  [19].

As  $N$  increases, we gradually observe in Fig. 1 the emergence of well-resolved above threshold ionization (ATI) peaks, while the directional asymmetry and interference pattern disappear—in other words, a distribution fully consistent with the photon picture. The fact that the asymmetry disappears may again be understood classically. For example, for  $N = 6, 7$ , the field takes almost a full revolution on the circle, corresponding to a monochromatic field with our field strength, and a preferred instant of ionization  $t_0$  cannot be clearly defined. There is almost an entire period around  $\frac{\pi}{2}$ , where the electron is equally likely to emerge into the continuum, leading to an angularly symmetric distribution, in agreement with Fig. 1.

#### B. Interference structures

The behavior of the interference features in Fig. 1 for  $N \leq 5$  can be understood by looking at the power spectrum of the pulse. Figure 3 shows the power spectrum for different values of  $N$ . The spectrum is very broad for  $N = 2, 4$ , with a lot of frequencies contributing with comparable magnitude. As a consequence there is a large number of different paths leading to the same final energy and such paths can interfere with each other. We see from Fig. 3 that the width of the spectrum for  $N = 2$  is  $\Delta\omega \sim 0.05$ , corresponding to  $\Delta E \sim 0.05$ . For a momentum of  $q = 0.67$  this corresponds to a huge shift in momentum of  $\Delta q \sim 0.07$ , which is clearly visible with our grid discretization. This explains the observed interference pattern in Fig. 1. The structure is simply caused by the fact that our pulse contains a very large number of frequencies when  $N$  is small (the pulse duration is small). As  $N$  increases the width of the spectrum gets smaller and frequencies close to  $\omega_0$  dominate completely. Thus we regain

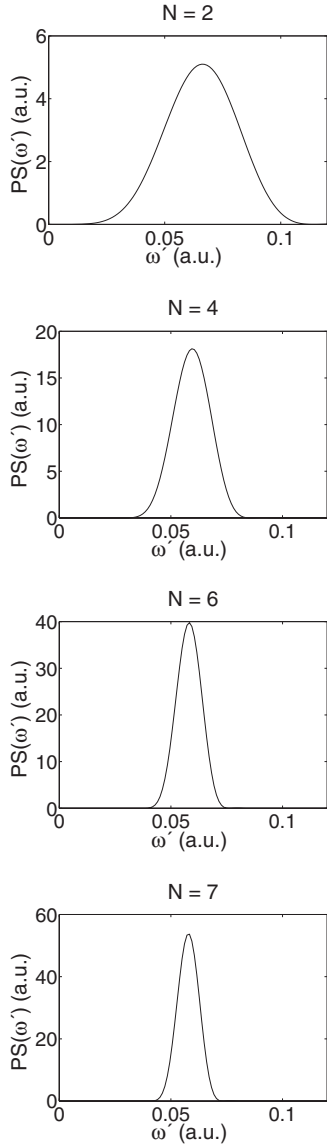


FIG. 3. Power spectrum  $|\int_{-\infty}^{\infty} E_x(t)e^{i\omega t} dt|^2 + |\int_{-\infty}^{\infty} E_y(t)e^{i\omega t} dt|^2$  of the electric field for four different values of  $N$ . The parameters are  $I=5.0 \times 10^{13}$  W/cm<sup>2</sup>,  $\omega_0=0.057$  (800 nm), and  $\phi=\pi/2$ .

the photon picture. For  $N=7$  we have  $\Delta\omega < 0.01$  which corresponds to  $\Delta q < 0.015$  for  $q=0.67$ . This explains why the interference pattern disappears and why we observe well-resolved ATI peaks as  $N$  increases.

The spectrum of the pulse depends on the form of the envelope. It is therefore interesting to examine if we obtain the same effects with a different envelope. We have calculated the momentum distribution using a Gaussian envelope,  $f(t)=\exp[-(t-\tau/2)^2/\tau_p^2]$ , with  $\tau_p=2 \arccos(2^{-1/4})\tau/\pi$  [16], and confirmed the interference effects reported above. The width of the spectrum for a pulse with a Gaussian envelope is a bit smaller for a given value of  $N$ , which leads to small changes.

### C. Saddle-point method

In addition to the SFA we use the SPM of Eq. (3) to calculate the time integral in Eq. (1). The results of such

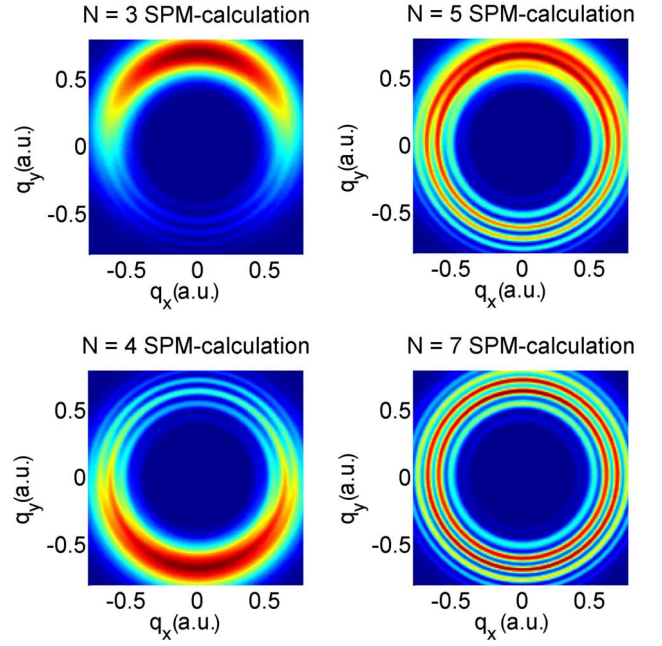


FIG. 4. (Color online) Momentum distribution  $(q_x, q_y)$  as predicted by the saddle-point method (SPM) using Eqs. (3) and (2), in the plane of polarization of the right-hand circularly polarized field  $\vec{E}$  propagating in the  $z$  direction for strong-field ionization of H(1s) for various values of  $N$ , with  $I=5.0 \times 10^{13}$  W/cm<sup>2</sup>,  $\omega_0=0.057$  (800 nm), and  $\phi=\pi/2$ . The grid size is  $\Delta q_x=\Delta q_y=0.01$ .

calculations are shown in Fig. 4, with  $I=5.0 \times 10^{13}$  W/cm<sup>2</sup>,  $\omega_0=0.057$ , and  $\phi=\pi/2$ . The saddle-point equation is solved using a modified Newton-Raphson method [30]. The probability amplitude is then calculated using Eq. (3). From Fig. 4, we see that there is good agreement between the results obtained by an exact numerical integration of Eq. (1) (Fig. 1) and the results obtained by the SPM for  $N \geq 5$ . For smaller  $N$ , however, there are some serious discrepancies. The interference structure shown in Fig. 1 is completely absent in Fig. 4. The SPM gives a smooth distribution, without any interference pattern. This feature can be understood by looking at the solutions  $t_s$  to the saddle-point equation (4) and the associated amplitudes  $a_s(t_s)$ . Figure 5 shows an example of such solutions for two different values of  $N$ . There are three solutions to the saddle-point equation for  $N=2$  (upper panel), but the solution with the smallest imaginary part completely dominates the sum in Eq. (3) in regions with high yield. Since we need at least two solutions with comparable amplitudes to create a momentum distribution with an interference pattern, this explains why the interference pattern is missing in the SPM calculation for  $N=2$ . In the  $N=7$  case we have eight solutions, and typically 2/3 of them have comparable amplitudes. Then the sum in Eq. (3) contains interference terms and the SPM calculation gives a momentum distribution with well-developed peaks. The agreement between the SPM and the SFA does not improve by expanding  $S'$  as well as  $S$  to second order [31].

### D. Asymmetry in different models

Now let us briefly return to the question of CEPD effects in the momentum distribution. Spatial asymmetry in the ion-

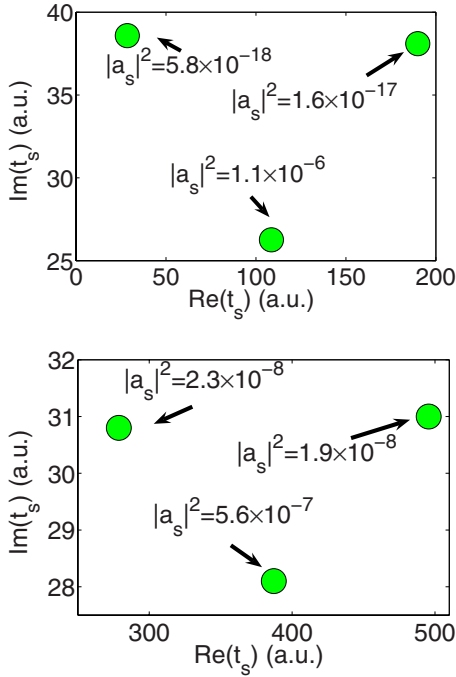


FIG. 5. (Color online) The complex instants of time  $t_s$  that solve the saddle-point equation (4) for  $N=2$  (upper panel) and  $N=7$  (lower panel). For  $N=7$ , only the three most dominant are shown. The number attached to the  $t_s$  solutions give the norm square of the amplitude  $a_s$  Eq. (3). The parameters are  $(q_x, q_y, q_z) \sim (0.0, -0.7, 0.0)$  (upper panel)  $(q_x, q_y, q_z) \sim (0.0, 0.7, 0.0)$  (lower panel),  $I = 5.0 \times 10^{13}$  W/cm<sup>2</sup>,  $\omega_0 = 0.057$  (800 nm), and  $\phi = \pi/2$ .

ization process was predicted theoretically some time ago in [12,13] and first measured in Ref. [14]. A detailed analysis of the latter experiment in terms of the SFA was given in Ref. [15]. Here we compare the SFA with the SPM. We define the following measure of asymmetry in the distribution [17]:

$$A(\theta_0) = \frac{|P_{\uparrow} - P_{\downarrow}|}{P_{\uparrow} + P_{\downarrow}}, \quad (6)$$

where  $P_{\uparrow}$  ( $P_{\downarrow}$ ) is the probability for ionizing in the direction  $0 < \theta < \theta_0$  ( $180^\circ - \theta_0 < \theta < 180^\circ$ ). In order to calculate  $P_{\uparrow}$  ( $P_{\downarrow}$ ) we first calculate  $dP/(dq_x dq_y)$ , using Eqs. (1) and (2), on a square grid  $[-0.8, 0.8]^2$  with grid size  $\Delta q_x = \Delta q_y = 0.01$ . When  $dP/(dq_x dq_y)$  is known on the grid  $P_{\uparrow}$  ( $P_{\downarrow}$ ) is calculated by summing up the appropriate momentum components. Figure 6 shows  $A(15^\circ)$  as a function of the number of optical cycles,  $N$ , for the two different approximations used in the article (SFA with Volkov wave function and SPM). There is a good agreement between the different approximations for  $N \geq 5$ , and  $A(15^\circ)$  becomes small for increasing  $N$  as expected. The situation is quite different for  $N \in \{2, 3\}$ , where  $A_{\text{SPM}}(15^\circ)$  increases as  $N$  decreases, while  $A_{\text{SFA}}(15^\circ)$  decreases as  $N$  decreases.  $A_{\text{SFA}}(15^\circ)$  has a maximum at  $N = 3, 4$ . We have checked that this conclusion is independent of  $\theta_0$ . The nonmonotonic behavior of  $A(15^\circ)$  was also observed and explained for a linear polarized laser pulse in Ref. [16]. However, the physics behind the nonmonotonic behavior is quite different in the two cases. While the asymmetry

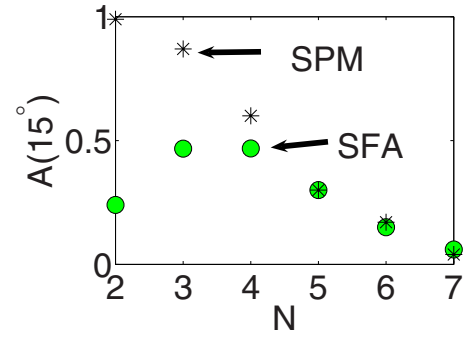


FIG. 6. (Color online)  $A(\theta_0=15^\circ)$  from Eq. (6) as a function of the number of optical cycles. The parameters are  $I=5.0 \times 10^{13}$  W/cm<sup>2</sup>,  $\omega_0=0.057$  (800 nm), and  $\phi=\pi/2$ . In the figure SPM denotes results obtained using the saddle-point method of Eq. (3). SFA denotes results obtained evaluating Eq. (1) by numerical integration.

for a linearly polarized pulse comes from the fact that such a pulse contains a number of well-localized extrema, a circularly polarized pulse contains only a single rather broad field maximum. From a purely classical point of view we would for circularly polarized light expect  $A(15^\circ)$  to increase as  $N$  decreases. The SPM predicts the same and is in that sense too classical: it overestimates the saddle-point close to the real time axis [ $\text{Im}(t_s)=0$ ].

#### IV. CONCLUSION

In this paper, we investigated bandwidth and CEPD effects in strong-field few-cycle ionization of atomic hydrogen. We studied the momentum distribution and observed a very complicated interference pattern in the case of a very short pulse ( $N < 5$ ). These interference effects disappear as the number of optical cycles increases, and we gradually observed the emergence of well resolved ATI peaks. A very short pulse contains a lot of different frequencies, which explains the observed interference pattern. The center frequency  $\omega_0$  begins to dominate as  $N$  increases, and we regain the normal photon picture. A very popular model, within the SFA, is the saddle-point method. For  $N > 4$ , we saw good agreement between the exact numerical integration and the saddle-point method. However, for  $N \leq 4$  the saddle-point method cannot describe the observed bandwidth effects since it overestimates the dominant saddle point for  $N$  small. Accordingly, the interferences observed in the electron momentum distribution cannot be associated with interference between ionization pathways leading to the same final state from different (complex) instants of ionization provided by the  $t_s$ 's. Also the SPM does not reproduce the maximum in the asymmetry of the momentum distribution obtained for  $N=3, 4$ .

#### ACKNOWLEDGMENT

This work was supported by the Danish Research Agency (Grant No. 2117-0 5-0081).

- [1] A. Scrinzi, M. Y. Ivanov, R. Kienberger, and D. M. Villeneuve, *J. Phys. B* **39**, R1 (2006).
- [2] A. H. Zewail, *J. Phys. Chem. A* **104**, 5660 (2000).
- [3] P. H. Buckbaum, *Nature (London)* **421**, 593 (2003).
- [4] M. Hentschel, R. Kienberger, C. Spielmann, G. A. Reider, N. Milosevic, T. Brabec, P. Corkum, U. Heinzmann, M. Drescher, and F. Krausz, *Nature (London)* **414**, 509 (2001).
- [5] M. Drescher, M. Hentschel, R. Kienberger, M. Uiberacker, V. Yakovlev, A. Scrinzi, T. Westerwalbesloh, U. Kleineberg, U. Heinzmann, and F. Krausz, *Nature (London)* **419**, 803 (2002).
- [6] T. Remetter, P. Johnsson, J. Mauritsson, K. Varjú, Y. Ni, F. Lépine, E. Gustafsson, M. Kling, J. Khan, R. López-Martens, *et al.*, *Nat. Phys.* **2**, 323 (2006).
- [7] S. Baker, J. S. Robinson, C. A. Haworth, H. Teng, R. A. Smith, C. C. Chirilă, M. Lein, J. W. G. Tisch, and J. P. Marangos, *Science* **312**, 424 (2006).
- [8] J. Itatani, J. Levesque, D. Zeidler, H. Nikura, H. Pépin, J. C. Kieffer, P. B. Corkum, and D. M. Villeneuve, *Nature (London)* **432**, 867 (2004).
- [9] M. F. Kling, C. Siedschlag, A. J. Verhoef, J. I. Khan, M. Schultze, T. Uphues, Y. Ni, M. Uiberacker, M. Drecher, F. Krausz, *et al.*, *Science* **312**, 246 (2006).
- [10] X. M. Tong and C. D. Lin, *Phys. Rev. Lett.* **98**, 123002 (2007).
- [11] V. Roudnev, B. D. Esry, and I. Ben-Itzhak, *Phys. Rev. Lett.* **93**, 163601 (2004).
- [12] E. Cormier and P. Lambropoulos, *Eur. Phys. J. D* **2**, 15 (1998).
- [13] P. Dietrich, F. Krausz, and P. B. Corkum, *Opt. Lett.* **25**, 16 (2000).
- [14] G. G. Paulus, F. Grasbon, H. Walther, P. Villorresi, M. Nisoli, S. Stagira, E. Priori, and S. D. Silvestri, *Nature (London)* **414**, 182 (2001).
- [15] D. B. Milošević, G. G. Paulus, and W. Becker, *Phys. Rev. Lett.* **89**, 153001 (2002).
- [16] S. Chelkowski and A. D. Bandrauk, *Phys. Rev. A* **65**, 061802(R) (2002).
- [17] S. Chelkowski and A. D. Bandrauk, *Phys. Rev. A* **71**, 053815 (2005).
- [18] D. B. Milošević, G. G. Paulus, and W. Becker, *Phys. Rev. A* **71**, 061404(R) (2005).
- [19] C. P. J. Martiny and L. B. Madsen, *Phys. Rev. Lett.* **97**, 093001 (2006).
- [20] D. B. Milošević, G. G. Paulus, D. Bauer, and W. Becker, *J. Phys. B* **39**, R203 (2006).
- [21] L. V. Keldysh, *J. Exp. Theor. Phys.* **47**, 1945 (1964).
- [22] F. H. M. Faisal, *J. Phys. B* **6**, L89 (1973).
- [23] H. R. Reiss, *Phys. Rev. A* **22**, 1786 (1980).
- [24] M. Lewenstein, P. Balcou, M. Y. Ivanov, A. L'Huillier, and P. B. Corkum, *Phys. Rev. A* **49**, 2117 (1994).
- [25] F. H. M. Faisal, *J. Phys. B* **40**, F145 (2007).
- [26] F. H. M. Faisal, *Phys. Rev. A* **75**, 063412 (2007).
- [27] D. Bauer, D. B. Milošević, and W. Becker, *Phys. Rev. A* **72**, 023415 (2005).
- [28] T. K. Kjeldsen and L. B. Madsen, *J. Phys. B* **37**, 2033 (2004).
- [29] C. B. Madsen and L. B. Madsen, *Phys. Rev. A* **74**, 023403 (2006).
- [30] W. H. Press, S. A. Teukolsky, W. T. Vetterling, and B. P. Flannery, *Numerical Recipes* (Cambridge University Press, Cambridge, England, 1992).
- [31] T. K. Kjeldsen and L. B. Madsen, *Phys. Rev. A* **74**, 023407 (2006).